Research Article / Review Article FUPRE JOURNAL 8(4):38-51(2024)

FUPRE Journal

of

Scientific and Industrial Research

ISSN: 2579-1184(Print) ISSN: 2578-1129 (Online)

http://fupre.edu.ng/journal

DFT-based Investigation of Physical Properties of LiYSn and LiScSn for Photovoltaic and Optoelectronic Applications

OTUEBE, A. Z.[1], *OMAGBEMI, A. A.*[1] *NENUWE N. O.*[1,*]

[1]*Department of Physics, Federal University of Petroleum Resources Effurun, Nigeria.*

ARTICLE INFO

Received: 04/04/2024
Accepted: 21/09/2024

Keywords

Half Heusler,
LiYSn,
LiScSn,
Photovoltaic,
Optical properties

ABSTRACT

An investigation is conducted on the characteristics of LiScSn and LiYSn half Heusler materials for their potential application as future photovoltaic materials. We provide an analysis of the structural, electronic, mechanical, and optical characteristics of the Li-based half Heuslers. These compounds have favourable electronic and optical properties, suggesting their potential value in photovoltaic and other optoelectronic applications. Density functional theory (DFT) has been extensively used to investigate and accurately characterize several aspects of condensed matter systems by computer simulations of electronic structure and optical characteristics. The structural optimization, energy band structure, density of states, and optical properties for these compounds are investigated using the exchange-correlation potential PBE-GGA and TB-mBJ techniques, implemented in the WIEN2k algorithm. The optical character of the compounds is determined by analyzing the components of the real and imaginary dielectric function, as well as the optical absorption, and refractive index.

1. INTRODUCTION

Semiconducting materials have received significant attention in recent years due to their superior technical applications in optoelectronic characteristics, solar irradiation, and photovoltaic irradiation processes. Heusler materials are frequently employed in spintronics, magnetic tunnel junctions, shape memory effects, electro-optic and optoelectronic devices such as sensors, magneto resistors, photovoltaic detectors, and light emitting diodes. Heusler alloys play a significant role in the quest for innovative materials with superior optical and electrical properties because of their broad band gap, huge magnetisation, and high Curie temperature (Khatri & Adhikari, 2024; Osafile & Nenuwe, 2021). Half Heusler (HH) materials with the XYZ composition (Y & X are transition elements; Z: sp-element) are a new structural version of the Heusler compound family that crystallize in the $C1_b$ crystal structure within F-43m symmetry and have lately gained attention (Khatri & Adhikari, 2024; Nenuwe & Umukoro, 2023; Nenuwe & Omagbemi, 2022; Yadav & Sanyal, 2015). The scientific community has struggled to identify semiconducting Heusler materials. Li-based Heusler materials have received a lot of attention among semiconducting Heusler compounds because of their potential use in linear optical and photonic applications due to photon absorption by the interband transition.

The Li-based half-Heuslers have garnered considerable interest as potential semiconductors for high-efficiency power electronic devices. This is mostly due to their many optical properties, such as high absorption coefficients and adjustable band gap energies, as well as their long-term stability. Half Heusler alloys belong to the category of semiconducting materials that exhibit a fully optical response. In addition to the many technical uses, the underlying physics of power electronic materials is equally abundant and captivating. Given the technological

*Corresponding author, e-mail:nenuwe.nelson@fupre.edu.ng
DIO

significance of these compounds, it is essential to understand their structural, electronic, optical, and elastic properties. This study primarily aims to investigate and analyse these properties.

Yadav and his colleagues (Yadav & Sanyal, 2015) calculated the thermoelectric properties of half Heusler compounds with 8 valence electrons, studying their features of semiconductor and metallic reactivity. The spin-polarized computations for the half metallic Li-based half Heuslers, LiMnN, LiMnSi, and LiMnP were conducted by Damewood et al (2015). Kandpal et al. (2006) examined the band gap and bonding characteristics of many half Heusler compounds, such as LiMgN, LiMgAs, LiMgP, LiMgBi, LiAlSi, LiCdP, and LiZnP with valence electron counts ranging from 8 to 18. Kuriyama et al. (Kuriyama et al., 1994; Kuriyama & Katoh, 1988) investigated the optical band gap and electrical resistivity of half-Heusler alloys consisting of LiZnP and LiZnAs. LiZnAs and LiZnP were identified as wide-band semiconductors, with band gaps of 1.51 and 2.04 electron volts, respectively.
Bacewicz and Ciszek(1988) synthesised a LiZnAs crystal using the direct fusion method. The research revealed that LiZnAs is a P-type semiconductor with a band gap of 2.1 eV. Kacimi et al. conducted a study on the optoelectronic applications of group I–II–V and I–III–IV half-Heuslers using DFT calculations (Kacimi et al., 2014).Gruhn (2010) conducted a density functional theory analysis on eight-valence electron half-Heuslers XYZ and determined the lattice constants of 648 half-Heusler compounds. Among the I-III-IV compounds investigated, they predicted the lattice constants of LiYSn and LiScSn to be 6.58 and 6.33 Å, respectively.

It appears that only lattice constant of LiScSn and LiYSn have been predicted (Gruhn, 2010), and no comprehensive Ab initio investigation on LiScSn and LiYSn in all three structural phases (α, β, and γ) of the $C1_b$ structure has been conducted to the best of our knowledge. Therefore, studying the structure, electronic, mechanical, and optical characteristics of these Li-based half Heuslers in three atomic configurations, new possibilities can be explored for the advancement of photonic sensors and possible power electronic devices. This work presents a first principles study that analyses the structure, electronic, mechanical, and optical properties of the half-Heusler compounds LiScSn and LiYSn. We employed density functional theory (DFT) computations configured in WIEN2K software to determine the essential properties of LiScSn and LiYSn.

2. MATERIALS AND METHODS

The full potential linearized augmented plane wave (FP-LAPW) approach (Blaha et al., 1990), implemented in the WIEN2k code (Blaha et al., 2001), was employed to perform density functional theory (DFT) (Kepple & Griem, 1968) calculations on the half-Heuslers LiYSn and LiScSn alloys. The Kohn-Sham (KS) equation (Olovsson et al., 2009) employs the Perdew-Burke-Ernzerhof (PBE) (Perdew et al., 1996) functional to calculate the exchange-correlation (XC) potential. In our computations, we employ non-spin-polarized density functional theory to accurately consider the optimisation of electronic structures since LiYSn and LiScSn are non-magnetic materials. The energy convergence threshold was set to 10^{-5} Rydberg, whereas the charge convergence threshold was set at 10^{-4} e, where e represents the charge of an electron. The value of $R_{MT}K_{max}$ was assigned as 8 for the alloys to restrict the quantity of plane waves. Here, R_{MT} represents the Muffin-Tin Radius and K_{max} denotes the highest value chosen for the expansion of the entire plane wave vector. The R_{MT} values of Li, Y, and Sn were 1.85, 2.5, and 2.5 for LiYSn, and R_{MT} values of Li, Sc, and Sn were 1.85, 2.19, and 2.3, respectively for LiScSn. The conventional tetrahedron method (Jepson & Anderson, 1993) was employed to perform the integration over the Brillouin zone. In order to obtain accurate bandgap, we thoroughly analysed the electronic properties of LiYSn and LiScSn using the Tran-Blaha-modified Becke-John (TB-mBJ) approximation. Finally, the IRelast package (Jamal et al., 2018) implemented in WIEN2k was employed to evaluate the elastic constants

and mechanical properties of the compounds LiYSn and LiScSn.

3. RESULTS AND DISCUSSION

3.1 Structural Stability

The equilibrium lattice constants of LiScSn and LiYSn were obtained by optimizing the total energy of each compound at their respective equilibrium volumes using Murnaghan's equation of state (see Eq. (1)) (Murnaghan, 1944). The computation was performed for each compound in its cubic structure, which corresponds to space group 216 (F-43m). Three types of phases were considered, each corresponding to distinct Wyckoff positions held by different atoms in each compound. Table 1 displays the Wyckoff positions for various cubic configurations of half-Heuslers. Figure 1 demonstrates the crystal structures of HHs LiScSn and LiYSn, which are of the cubic type α and type β, respectively. Each of the Sn-atom is bonded to both Sc and Li atoms, while the Li atoms are located between two atoms of Sc in type α phase for LiScSn (see Figure 1(a)). In Figure 1(b), each of the Li-atom is bonded to Sn and Y atoms, while the Sn atoms lie between two atoms of Y for LiYSn in type β.

$$E_T(V) = E_0 + \frac{B_0 V}{B_0'(B_0'-1)}\left\{\left(\left(\frac{V_0}{V}\right)^{B_0'} - 1\right) + B_0'\left(1 - \frac{V_0}{V}\right)\right\} \quad (1)$$

where E_0, V_0, B_0, & B_0' have their traditional meanings. The optimized lattice constants (a_0), minimum energies E_0, bulk modulus (B_0), and its pressure derivative (B_0') for LiScSn and LiYSn in the non-magnetic (NM) configuration, which are reported in Table 2, were determined by Eq. (1).

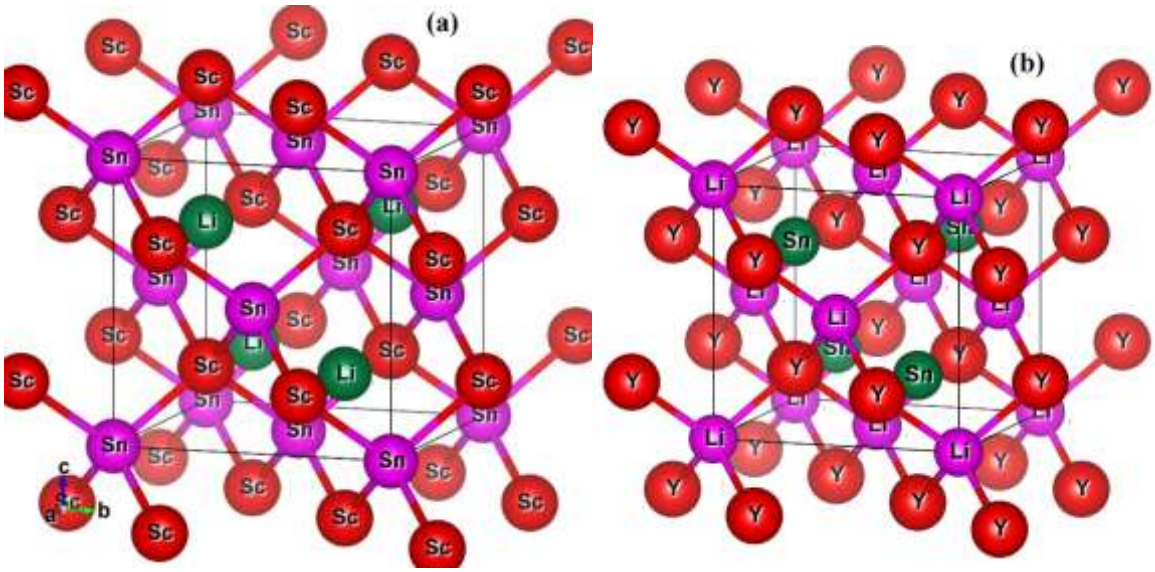

Figure 1. Crystal structure of (a) LiScSn in phase type α and (b) LiYSn in phase type β.

Table 1: Nonidentical site occupancy within a cubic structure for half-Heusler.

Phase	Atom		
	Li	**Sc/Y**	**Sn**
Type α	(0.25, 0.25, 0.25)	(0.75, 0.75, 0.75)	(0, 0, 0)
Type β	(0, 0, 0)	(0.75, 0.75, 0.75)	(0.25, 0.25, 0.25)
Type γ	0.5, 0.5, 0.5	(0.75, 0.75, 0.75)	(0, 0, 0)

Table 2. Calculated equilibrium volume V_0 (bohr^3), lattice constants a_0 (Å), total energies E_0 (Ry), bulk modulus B_0 (GPa), its pressure derivative B_0', formation energy E_f(Ry), and band gap E_g(eV) for LiYSn in the non-magnetic state.

Alloy	Phase	V_0	a_0	E_0	B	B'	E_f	E_g
	Type α	580.8140	7.0086	-19144.850519	38.9575	3.8609	-	-
LiYSn	Type β	481.2408	6.5828	-19144.857167	47.5859	4.0914	-0.015855	$0.942^{\text{TB-mBJ}}$ $0.736^{\text{GGA-PBE}}$
	Type γ	600.5729	7.0872	-19144.763560	34.8636	3.3617	-	-
	Type α	511.7834	6.7192	-13901.857193	41.7149	3.8377	-0.006175	$0.881^{\text{TB-mBJ}}$ $0.664^{\text{GGA-PBE}}$
LiScSn	Type β	427.6103	6.3285	-13901.856372	50.3490	4.3829	-	-
	Type γ	521.5294	6.7616	-13901.788250	39.1066	3.4326	-	-

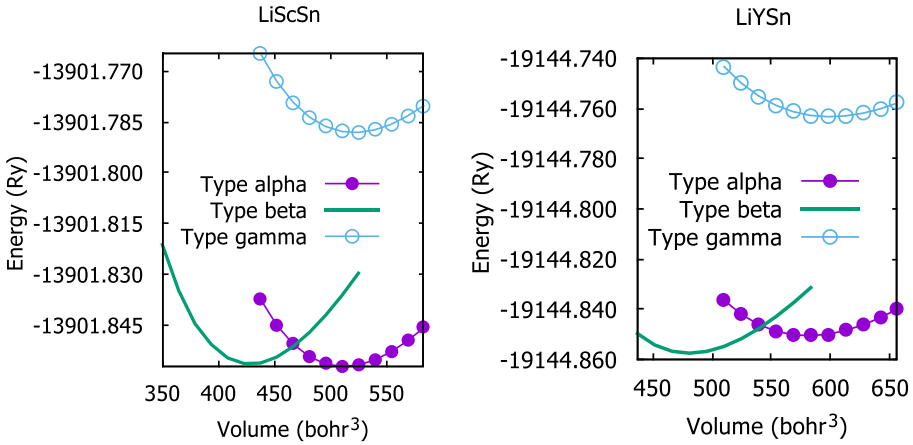

Figure 2. Murnaghan equation of state-fitted optimization curves for LiScSn and LiYSn in the non-magnetic state of type α, type β, and type γ

Figure 2 illustrates the relationship between volume and total energy change, as shown by the curves for type α, type β, and type γ in the non-magnetic configuration. According to our

findings, we discovered that the cubic structure type β has the lowest energy for the LiYSn, while the cubic structure type α has the minimum energy for the LiScSn alloy. This suggests that LiYSn is more stable in the non-magnetic state of type β, while LiScSn is more stable in phase type α in the non-magnetic state. The calculated results are presented in Table 2. The minimum energies obtained from our calculations for the alpha-type structure is -13901.857193 Ry for LiScSn and -19144.8571 Ry for the beta-type structure LiYSn. The lattice constants for LiScSn and LiYSn are 6.7192 Å and 6.583 Å, respectively. These findings have close agreement with the data obtained by Gruhn (2010), who conducted a comparative analysis of 648 compounds and determined the lattice constants of LiScSn and LiYSn to be 6.333 and 6.581 Å, respectively. The bulk modulus value obtained for each alloy is 41.71 GPa for LiScSn and 47.585GPa for LiYSn. The lattice constant of LiScSn is found to be greater than that of LiYSn. Conversely, the bulk modulus of LiYSn is greater than the bulk modulus of LiScSn. This indicates that the bulk modulus increases as the atomic number increases.

The formation energy (E_f) illustrates the chemical stability of the compound via (Wang et al., 2014).

$$\boldsymbol{E_f = \frac{E_T^{XYZ} - E_{Bulk}^{X} - E_{Bulk}^{Y} - E_{Bulk}^{Z}}{3}} \quad (\mathbf{2})$$

Where $\boldsymbol{E_T^{XYZ}}$ is the total energy in the cubic structure, and $\boldsymbol{E_{Bulk}^{X}}$, $\boldsymbol{E_{Bulk}^{Y}}$, & $\boldsymbol{E_{Bulk}^{Z}}$ are the energy of each atom in its bulk form. The obtained results by our calculations are -0.006175 Ry for LiScSn and -0.015855 Ry for LiYSn. It is observed that both values obtained for Ef are negative and confirm the potential for synthesizing these compounds experimentally. Due to the absence of both experimental data for comparison, we shall consider our findings as predictions for future research.

3.2 Mechanical Stability

The half-Heusler compounds LiScSn and LiYSn possess a cubic crystal structure. Consequently, the elastic characteristics of these compounds can be analysed by considering the elastic constants C_{11}, C_{12}, and C_{44} (Mehl, 1993; Schreiber et al., 1975). The IRelast (Jamal et al., 2014) technique configured in WIEN2K package was employed to evaluate the elastic and mechanical properties. The equations applied to define the mechanical stability conditions of the Born criterion (Born et al., 1955; Waller, 1956) for elastic constants related with cubic structure are

$$\boldsymbol{C_{11} > 0}, \quad \boldsymbol{C_{44} > 0}, \quad \boldsymbol{C_{11} > C_{12}}, \quad \boldsymbol{2C_{12} + C_{11} > 0} \quad (\mathbf{3})$$

The Cauchy pressure (Pettifor, 1992)

$$C' = C_{12} - C_{44} \quad (4)$$

The bulk modulus

$$B = \frac{C_{11} + 2C_{12}}{3} \quad (5)$$

The Zener anisotropy factor (Pan et al., 2018)

$$A = \frac{2C_{44}}{C_{11} - C_{12}} \quad (6)$$

G_V refers to the Voigt shear modulus, and G_R refers to the Reuss shear modulus by (Shrikanth et al., 2021)

$$G_V = \frac{C_{11} - C_{12} + 3C_{44}}{5} \quad (7)$$

G is shear modulus that indicates a resistance for a plastic deformation.

$$G = \frac{G_V + G_R}{2} \quad (9)$$

The Poisson's ratio v is given as

$$v = \frac{C_{12}}{C_{11} + C_{12}} \quad (10)$$

Young modulus E is given as

$$E = \frac{(C_{11} - C_{12})(C_{11} + 2C_{12})}{C_{11} + C_{12}} \quad (11)$$

The calculated results are displayed in Table 3. Based on the examination of the elastic constants C_{11}, C_{12} & C_{44} for each alloy in alpha and beta cubic structure, it is evident that the stability criteria, as defined by Eq. (3), are satisfied for LiScSn and LiYSn, respectively.

Table 3. Estimated elastic constant C_{ij}(GPa), bulk modulus *B* (GPa), Young modulus *E* (GPa), Cauchy pressure C'(GPa), shear modulus *G* (GPa), Poisson's ratio *v*, Pugh ratio *B/G* and Zener anisotropy factor *A* for LiScSn and LiYSn half-Heuslers.

Alloy	C_{11}	C_{12}	C_{44}	$C_{12} - C_{44}$	*B*	*E*	*G*	*v*	A	B/G
LiScSn	68.26	28.98	35.48	-6.51	42.07	68.72	27.99	0.228	1.80	1.503
LiYSn	63.40	26.22	31.76	-5.54	38.61	62.94	25.62	0.228	1.70	1.507

The bulk modulus values of LiScSn and LiYSn are 42.07 GPa and 38.61 GPa, respectively. The LiScSn alloy exhibits a greater bulk modulus and unidirectional compression in comparison to the LiYSn alloy. This attribute is a result of a significant elastic constant C_{11}. The calculated Cauchy pressure values are -6.51 for LiScSn and -5.54 for LiYSn. The Cauchy pressure values are negative, indicating a brittleness attribute arising from the atomic-level bonding nature. The Pugh's ratio B/G is a measure that characterizes the brittleness or ductility of a material. A value of 1.75 serves as the boundary between the two domains. According to the research published in Ref. (Butt et al., 2020) , an alloy exhibits brittle behaviour when its B/G ratio is less than 1.75. Conversely, if the B/G ratio exceeds this crucial value, the alloy demonstrates ductile behaviour. This study presents the B/G ratios of 1.503 and 1.507 for LiScSn and LiYSn, respectively. These results demonstrate the brittle nature of LiScSn and LiYSn. The anisotropy factor A quantifies the correlation between measurement taken in different directions. The study reported in (Zaman et al., 2021) defines a compound as isotropic when A is equal to 1, and anisotropic when A is not equal to 1. The computed results for LiScSn are 1.80, while for LiYSn they are 1.70. The results indicate that the values obtained for A in relation to the two alloys LiScSn and LiYSn are greater than one, implying that both compounds are anisotropic materials.

We conducted an investigation on Poisson's ratio (v) to determine its relationship with hardness. A material with a Poisson's ratio of 0.26 exhibits both ductile and brittle characteristics. The compound exhibits brittleness when the value of v is less than 0.26. Otherwise, it displays ductility (Mehmood et al., 2017). In this study, we have reported a value of 0.228 for both compounds. These obtained results confirm the brittle nature of LiScSn and LiYSn. Young's modulus quantifies a material's response to a linear deformation, and a high value of E signifies the material's rigidity. The determined values of the elastic modulus (E) for LiScSn and LiYSn are 68.72 GPa and 62.94 GPa, respectively. Therefore, we can deduce that LiScSn is the most rigid.

3.3 Electronic Properties

By closely examining the electronic features, we can make accurate predictions about the properties of materials and determine their specific uses. Here, we focused on analyzing the electronic characteristics by studying their band structure (BS), total density of states (TDOS), and partial density of states (PDOS).

3.3.1 The Band Structure

The band structures of LiScSn and LiYSn were examined utilizing the GGA-PBE and TB-mBJ methods. The use of TB-mBJ for predicting band gap values is known to yield accurate results that closely align with experimental measurements. Figures 3 showcases the band structures of LiScSn and LiYSn, including the high symmetry directions within the Brillouin zone. These results were obtained using the TB-mBJ method. Each curve depicts a band structure consisting of the conduction and valence bands, which are separated by the Fermi level. The conduction bands are situated in the top region, while the valence bands are positioned in the bottom region of the curve. The two zones are divided by the band gap that is intersected by the Fermi level. The calculations for LiScSn indicate that the valence band maximum (VBM) is situated on the gamma high-symmetry axis, while the conduction band minimum (CBM) is found along the X high-symmetry axis. This suggests that the LiScSn alloy is a semiconductor with an indirect band gap at the Γ-X point. This is similar to the results obtained for the α-phase of RuVBi by Nenuwe and co-worker (2023). The LiYSn material has a direct bandgap along X-X, since both the CBM and VBM are observed along the same high-symmetry axis X. This indicates that the LiYSn material is a direct bandgap semiconductor. Based on the predicted results presented in Table 2, utilizing GGA-PBE, the band gap measurements for LiScSn and LiYSn are determined to be 0.664 eV and 0.736 eV, respectively. The TB-MBJ method yields band gap values of 0.881 eV and 0.942 eV for LiScSn and LiYSn, respectively. The band gap values computed using TB-mBJ are greater than those obtained using GGA-PBE. The band structures obtained using the TB-mBJ method are depicted in Figure 3.

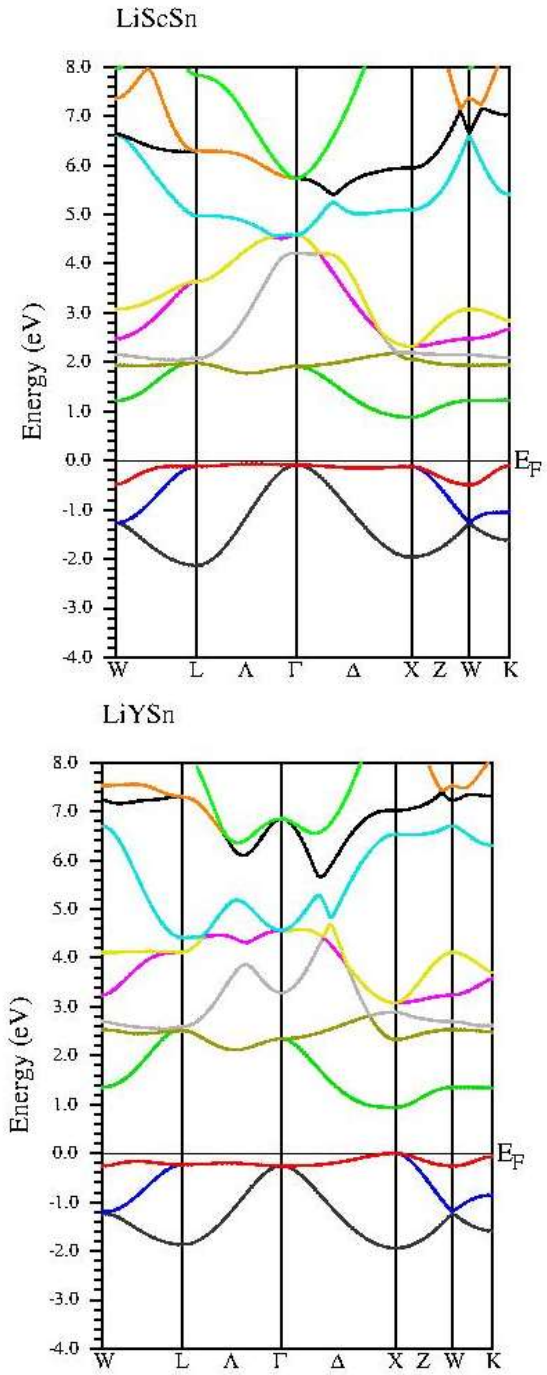

Figure 3. Band structure for LiScSn and LiYSn compounds

3.3.2 Total Density of States and Projected Density of States

The total density of states (TDOS) and partial density of states (PDOS) curves facilitate a clear representation of the configurations of distinct energy levels. Figures 4 and 5 depict the total and partial density of states for LiScSn and LiYSn alloys, respectively, as

obtained via the TB-mBJ method. Figure 4 shows the total density of states for LiScSn and LiYSn, where the contribution from each atom is clearly represented. The partial (or projected) density of states curves for *s*-Li, *d*-Y, *d*-Sc, and *p*-Sn exhibit a notable similarity in their shapes for both materials (see Figure 5). The resemblance is evident in the alignment of various peaks in the conduction and valence bands. The sharp spikes in the valence bands are a result of the mixing of 5*p*-Sn and 3*d*-Sc, 4*d*-Y states in both compounds. The majority states consist of 4*d*-Y, 3*d*-Sc and 5*p*-Sn, whereas the minority states are represented by 2s-Li. The Fermi level resides within an empty zone. This region referred to as the band gap is defined by the states resulting from the hybridization of 5*p*-Sn and 4*d*-Y, 3*d*-Sc states in the valence band, and 4*d*-Y, and 3*d*-Sc states in the conduction band. In the case of LiScSn, the highest point in the valence band is situated at -0.10667 eV, whereas the highest point in the conduction band is found at 1.934 eV. The energy gap ranges from 0.02 to 0.90 electron volts (eV). The highest peak in the valence band (VB) of LiYSn is found at -0.163 eV, whereas the highest peak in the conduction band (CB) is located at 2.47 eV. The energy gap is situated within the range of 0.027 to 0.97 electron volts (eV).

3.4 Optical Properties

Examining the optical characteristics of a material provides insights into how the material behaves when it is exposed to sunlight. The compounds LiScSn and LiYSn were analysed utilizing PBE-GGA exchange correlations via Wien2k to determine their optical properties, such as refractive index n (w), absorption coefficient α(w), and complex dielectric function ε(w). The dielectric function is a parameter used to analyze the interaction between the material and phonons, which is dependent on the energy of the photons. The dielectric function can be used to determine the optical response of a materials at different photon energies. The dielectric function is expressed as a complex quantity. Equation (12) represents the dielectric function ε(w) as the sum of two components (Khan et al., 1993):

$$\varepsilon(w) = \varepsilon_1(w) + i\varepsilon_2(w) \qquad (12)$$

where $\varepsilon_1(w)$ and $\varepsilon_2(w)$ are respectively the real and imaginary parts of the dielectric functions for LiScSn and LiYSn compounds.

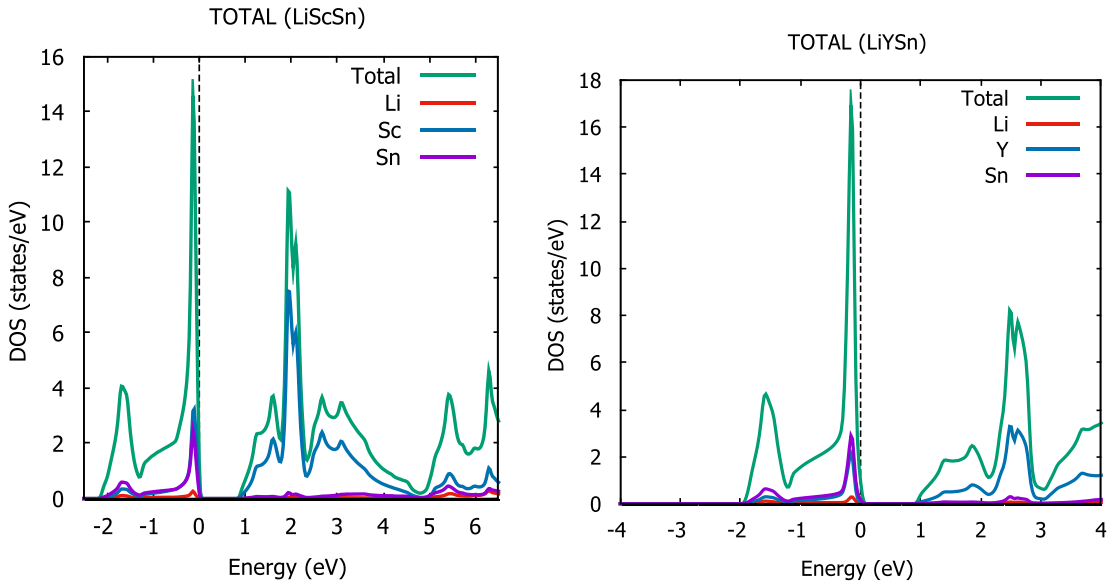

Figure 4 Total density of states for LiScSn and LiYSn

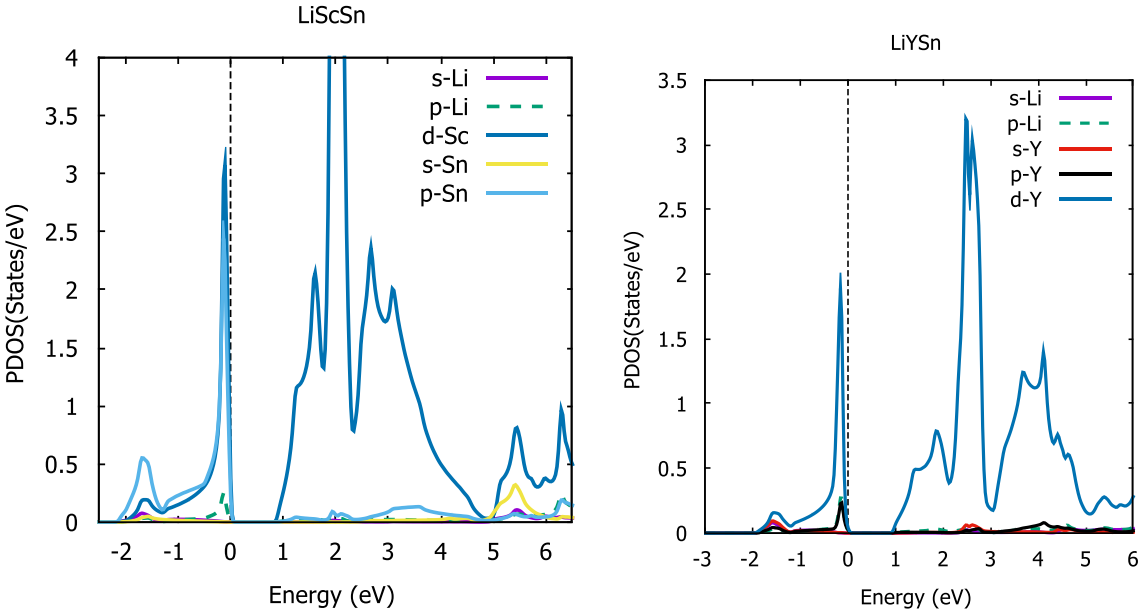

Figure 5 Partial density of states for LiScSn and LiYSn

3.4.1 The real part of the dielectric function

Figure 6 represents the variation in the real component of the dielectric function $\varepsilon_1(w)$ with respect to photon energy throughout the range of 0.01361 – 13.56488 eV. The plot illustrating the variation of $\varepsilon_1(w)$ for LiYSn is depicted by a continuous green line, while for LiScSn it is represented by a continuous violet line. The curve consists of two sections: the initial part represents the behaviour of the material at zero frequency, referred to as the static dielectric constant $\varepsilon_1(0)$, which corresponds to frequencies near to zero. The initial values of $\varepsilon_1(w)$ are 17.19 for LiScSn and 15.63 for LiYSn, as observed. The initial segment encompasses the internal energy range of 0 – 2.2994 eV for LiScSn and 0 – 2.81 eV for LiYSn. These energy intervals contain abrupt peaks that are associated with dispersion. The highest peak of $\varepsilon_1(w)$for LiScSn is located at 0.966 eV, while for LiYSn it is at 0.802 eV. The second part is located between the positions where the value of $\varepsilon_1(w)$ is negative. This region refers to the phenomenon of photon damping, which signifies the presence of metallic properties within a specific range of energy. This region is between 2.299 and 13.56 eV for LiScSn and between 2.81 and 13.56 eV for LiYSn. The minimum negative value of $\varepsilon_1(w)$ is achieved at 5.70 eV for LiScSn and at 2.92 eV for LiYSn.

3.4.2 The imaginary part of the dielectric function

The dielectric function $\varepsilon_2(w)$ is linked to the electronic absorption of a material. Figure 2 displays the imaginary component of the dielectric function $\varepsilon_2(w)$. It was observed that the absorption process starts at nearly zero energy for both LiScSn and LiYSn alloys. The zero energies for LiScSn and LiYSn correspond to frequencies of 0.42 and 0.38, respectively. These frequencies indicate the threshold values for these materials. The imaginary portion of the dielectric function $\varepsilon_2(w)$ represents the absorption of materials. Here, $\varepsilon_2(w)$ exhibits three absorption peaks at approximately 1.56 eV, 2.19 eV, and 5.45 eV, with a minimum at 13.56 eV for LiScSn. For LiYSn, the absorption peaks are located at approximately 1.83 eV, 2.76 eV, and 4.42 eV, with a minimum near 13.56 eV. The optical transition from Sn-5p bands to the Sc-3d (and Y-4d) conduction bands originates

these three peaks. The minimum near 13.56 eV reflects small energy gap in the conduction band region.

3.4.3 The Absorption Coefficient $\alpha(w)$

The absorption coefficient α(w) is a crucial parameter for analyzing the characteristics of photon energy beams as they traverse a material. The value of α(w) is determined by its imaginary component, which is computed using the following formula (Saim et al., 2022).

$$\boldsymbol{\alpha(w) = \frac{\sqrt{2w}}{c}\left[\left(\varepsilon_1^2(w) + \varepsilon_2^2(w)\right)^{\frac{1}{2}} - \varepsilon_1(w)\right]^{\frac{1}{2}}} \quad (13)$$

Where c is the speed of light. Figure 7 illustrates the absorption curves of LiScSn and LiYSn half-Heusler compounds. There are similarities between these two curves for $\alpha(w)$. It is observed that the absorption varies according to the increasing values of frequencies. The presence of several moderately acute peaks is recorded as the absorption increases to a maximum and then decreases with increasing energy. It can be seen from Figure 7 that the curve for LiScSn, the absorption maximum of the highest peak is at 148.85 x 10^4 cm^{-1} at 5.61 eV (221.03 nm). Between 0 eV to 5.61 eV are two smaller absorption peaks, the first one is positioned at 2.35 eV (527.65 nm) with absorption equal to 77.65 x 10^4 cm^{-1}, and the second is positioned at 4.26 eV (291.07 nm) with an absorption of 97.25 x 10^{-1} cm^{-1}. Beyond the maximum $\alpha(w)$, the absorption decreases almost rapidly to 68.89 x 10^4 cm^{-1} at 13.56 eV (91.44 nm).

For LiYSn in Figure 7, the $\alpha(w)$ increased almost rapidly to a peak of 102.6 x 10^4 cm^{-1} at 2.89 eV (429.06 nm), then decreased and increased rapidly to a maximum value of equal to 120.8 x 10^4 cm^{-1} at 4.83 eV (256. 72 nm). Beyond this point, $\alpha(w)$ varies with frequency and finally decreased to a minimum value equal to 54.65 x 10^4 cm^{-1} at 13.56 eV (91.44 nm). The results obtained indicate that the materials LiScSn and LiYSn absorb light in the ultraviolet range for the entire range of photon energies.

3.4.4 Refractive Index

The refractive index of a material is a crucial metric for photoelectric applications. The refractive indexes of LiScSn and LiYSn are displayed in Figure 8. The refractive indexes exhibit many peaks in the UV area and then gradually fall to a minimum value of 0.17 and 0.15 for LiScSn and LiYSn, respectively, at around 13.56 eV. The peaks originate from the interband transition between the highest valence band and the lowest conduction band. The presence of peaks in the UV range indicates that the refractive index exhibits non-linear characteristics.

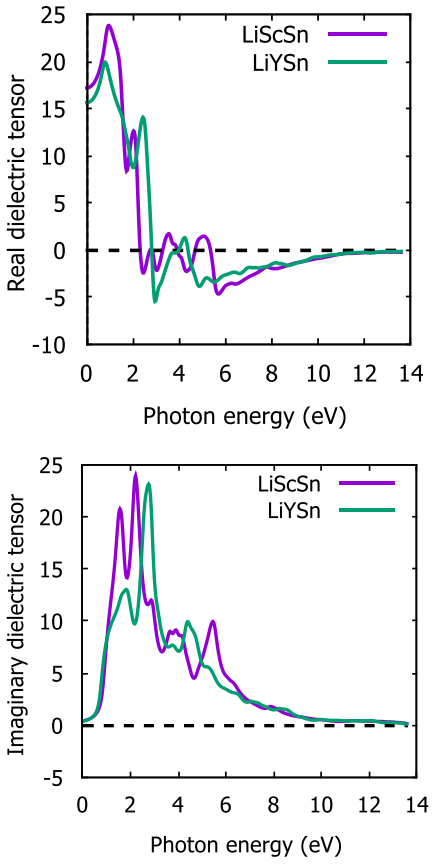

Figure 6. Real and Imaginary part of the dielectric function of LiScSn and LiYSn half-Heusler materials versus photon energy at their equilibrium lattice constants.

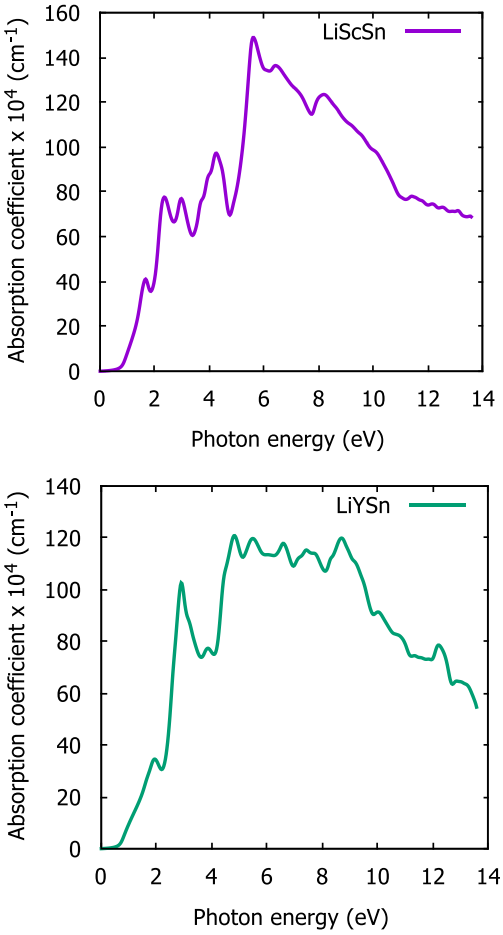

Figure 7. Absorption coefficient of LiScSn and LiYSn half-Heusler materials versus photon energy at their equilibrium lattice constants

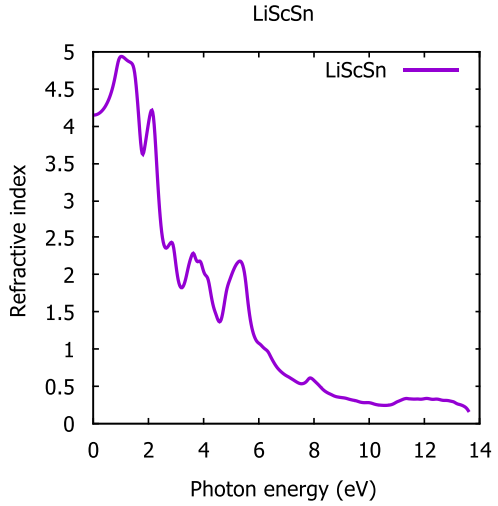

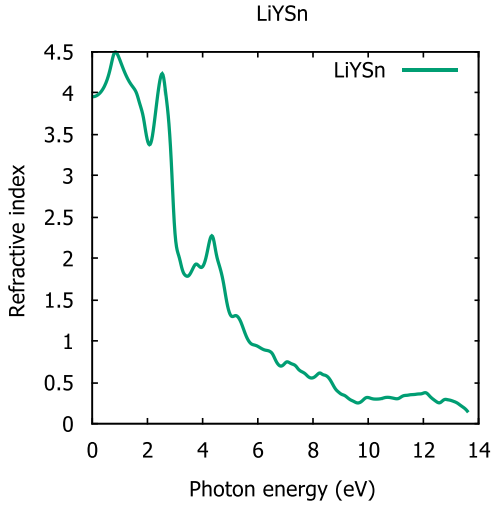

Figure 8. Refractive index of LiScSn and LiYSn half-Heusler materials versus photon energy at their equilibrium lattice constants.

4. CONCLUSION

In this research work, we have carried out a first principles calculation to investigate the structural, mechanical, electronic and optical properties of LiScSn and LiYSn half-Heusler compounds. In our calculation, we have used density functional investigations for Li-based half-Heusler of LiScSn and LiYSn which is performed by using the full potential linearized augmented plane wave (FP-LAPW) method, PBE-GGA and TB-mBJ methods as implemented in WIEN2k code. Then the electronic properties of the optimized state were examined such as bandgap energy, and the density of states (DOS). The optical properties such as real and imaginary dielectrics, refractive index and absorption coefficient were examined. The results for the structural property calculations indicate that LiYSn half-Heusler is stable in the cubic type β structure, while LiScSn is stable in the cubic type α structure in non-magnetic state. The values obtained for the lattice parameters is in agreement with available theoretical value. The mechanical property investigation showed that LiScSn and LiYSn obey the stability criteria. LiScSn and LiYSn were found to be brittle in nature. From the electronic properties, the semiconductor property of LiYSn was revealed, with a direct

bandgap along X-X point, while LiScSn was predicted as indirect bandgap along Γ-X symmetry point. In the band structure there is a band gap between the conduction band and the valance band with the Fermi level at the middle. Also, the DOS confirms the results obtained from the band structure. The optical properties revealed LiScSn and LiYSn compounds are good light absorbers in the ultraviolet range. Therefore, these half-Heuslers are promising materials for future photovoltaic and optoelectronic applications.

Acknowledgments

The author(s) acknowledge(s) the Editor in chief and the Reviewers for their selfless services to improve this research work.

References

Bacewicz, R., & Ciszek, T. F. (1988). Preparation and characterization of some AIBIIC V type semiconductors. *Applied Physics Letters*, *52*(14). https://doi.org/10.1063/1.99188.

Blaha, P., Schwarz, K., & Madsen, G. K. H. (2001). WIEN2K, An Augmented Plane Wave+ Local Orbitals Program for Calculating Crystal Properties (TU Wien, Austria, 2001). *Isbn 3-9501031-1-2*, *2*.

Blaha, P., Schwarz, K., Sorantin, P., & Trickey, S. B. (1990). Full-potential, linearized augmented plane wave programs for crystalline systems. *Computer Physics Communications*, *59*(2). https://doi.org/10.1016/0010-4655(90)90187-6.

Born, M., Huang, K., & Lax, M. (1955). Dynamical Theory of Crystal Lattices. *American Journal of Physics*, *23*(7). https://doi.org/10.1119/1.1934059.

Butt, M. K., Yaseen, M., Bhatti, I. A., Iqbal, J., Misbah, Murtaza, A., Iqbal, M., AL-Anazy, M. mana, Alhossainy, M. H., & Laref, A. (2020). A DFT study of structural, magnetic, elastic and optoelectronic properties of lanthanide based XAlO3 (X=Nd, Gd) compounds. *Journal of Materials Research and Technology*, *9*(6). https://doi.org/10.1016/j.jmrt.2020.11.055.

Damewood, L., Busemeyer, B., Shaughnessy, M., Fong, C. Y., Yang, L. H., & Felser, C. (2015). Stabilizing and increasing the magnetic moment of half-metals: The role of Li in half-Heusler LiMnZ (Z=N,P,Si). *Physical Review B - Condensed Matter and Materials Physics*, *91*(6). https://doi.org/10.1103/PhysRevB.91.064409.

Gruhn, T. (2010). Comparative ab initio study of half-Heusler compounds for optoelectronic applications. *Physical Review B - Condensed Matter and Materials Physics*, *82*(12). https://doi.org/10.1103/PhysRevB.82.125210.

Jamal, M., Bilal, M., Ahmad, I., & Jalali-Asadabadi, S. (2018). IRelast package. *Journal of Alloys and Compounds*, *735*. https://doi.org/10.1016/j.jallcom.2017.10.139.

Jamal, M., Jalali Asadabadi, S., Ahmad, I., & Rahnamaye Aliabad, H. A. (2014). Elastic constants of cubic crystals. *Computational Materials Science*, *95*. https://doi.org/10.1016/j.commatsci.2014.08.027.

Jepson, O., & Anderson, O. K. (1993). The electronic structure of h.c.p. Ytterbium. *Solid State Communications*, *88*(11–12). https://doi.org/10.1016/0038-1098(93)90260-T.

Kacimi, S., Mehnane, H., & Zaoui, A. (2014). I-II-V and I-III-IV half-Heusler compounds for optoelectronic applications: Comparative ab initio study. *Journal of Alloys and Compounds*, *587*. https://doi.org/10.1016/j.jallcom.2013.10.046.

Kandpal, H. C., Felser, C., & Seshadri, R. (2006). Covalent bonding and the nature of band gaps in some half-Heusler compounds. *Journal of Physics D: Applied Physics*, *39*(5). https://doi.org/10.1088/0022-3727/39/5/S02.

Kepple, P., & Griem, H. R. (1968). Improved stark profile calculations for the hydrogen lines Hα, Hβ, Hγ, and Hδ. *Physical Review*, *173*(1). https://doi.org/10.1103/PhysRev.173.317.

Khan, M. A., Kashyap, A., Solanki, A. K., Nautiyal, T., & Auluck, S. (1993). Interband optical properties of Ni3Al. *Physical Review B*, *48*(23). https://doi.org/10.1103/PhysRevB.48.16974.

Khatri, P., & Adhikari, N. P. (2024). Mechanical and thermoelectric response of 18-valence electron half-Heusler tellurides XFeTe (X=Ti, Hf): A theoretical perspective. *Materials Today Communications*, *39*. https://doi.org/10.1016/j.mtcomm.2024.108853.

Kuriyama, K., Kato, T., & Kawada, K. (1994). Optical band gap of the filled tetrahedral semiconductor LiZnAs. *Physical Review B*, *49*(16). https://doi.org/10.1103/PhysRevB.49.11452.

Kuriyama, K., & Katoh, T. (1988). Optical band gap of the filled tetrahedral semiconductor LiZnP. *Physical Review B*, *37*(12). https://doi.org/10.1103/PhysRevB.37.7140.

Mehl, M. J. (1993). Pressure dependence of the elastic moduli in aluminum-rich Al-Li compounds. *Physical Review B*, *47*(5). https://doi.org/10.1103/PhysRevB.47.2493.

Mehmood, N., Ahmad, R., & Murtaza, G. (2017). Ab Initio Investigations of Structural, Elastic, Mechanical, Electronic, Magnetic, and Optical Properties of Half-Heusler Compounds RhCrZ (Z = Si, Ge). *Journal of Superconductivity and Novel Magnetism*, *30*(9). https://doi.org/10.1007/s10948-017-4051-3.

Murnaghan, F. D. (1944). The Compressibility of Media under Extreme Pressures. *Proceedings of the National Academy of Sciences*, *30*(9). https://doi.org/10.1073/pnas.30.9.244

Nenuwe, N. O. (2023). TB-mBJ Predictions of Thermoelectric and Optical Properties of Half-Heusler RuVBi alloy. *Journal Research Article / Review Article FUPRE JOURNAL*, *7*(1), 55–70. http://fupre.edu.ng/journal.

Nenuwe, O. N., & Omagbemi, O. (2022). Electronic, thermodynamic, and effect of pressure on mechanical properties in CoTiSb and CoTiBi semi-Heuslers. *FUPRE Journal of Scientific and Industrial Research (FJSIR)*, *6*(4), 118–136 https://fupre.edu.ng/journal.

Olovsson, W., Tanaka, I., Puschnig, P., & Ambrosch-Draxl, C. (2009). Near-edge structures from first principles all-electron Bethe-Salpeter equation

calculations. *Journal of Physics Condensed Matter*, *21*(10). https://doi.org/10.1088/0953-8984/21/10/104205.

Osafile, O. E., & Nenuwe, O. N. (2021). Lattice dynamics and thermodynamic responses of XNbSn half-heusler semiconductors: A first-principles approach. *Journal of the Nigerian Society of Physical Sciences*, *3*(2). https://doi.org/10.46481/jnsps.2021.174.

Pan, Y., Wang, S. L., & Zhang, C. M. (2018). Ab-initio investigation of structure and mechanical properties of PtAlTM ternary alloy. *Vacuum*, *151*. https://doi.org/10.1016/j.vacuum.2018.02.027.

Perdew, J. P., Burke, K., & Ernzerhof, M. (1996). Generalized gradient approximation made simple. *Physical Review Letters*, *77*(18). https://doi.org/10.1103/PhysRevLett.77.3865.

Pettifor, D. G. (1992). Theoretical predictions of structure and related properties of intermetallics. *Materials Science and Technology (United Kingdom)*, *8*(4). https://doi.org/10.1179/mst.1992.8.4.345.

Saim, A., Belkharroubi, F., Boufadi, F. Z., Ameri, I., Blaha, L. F., Tebboune, A., Belkaid, M. N., Belkilali, W., Ameri, M., Al-Douri, Y., & Abd El-Rehim, A. F. (2022). Investigation of the Structural, Elastic, Electronic, and Optical Properties of Half-Heusler CaMgZ (Z = C, Si, Ge, Sn, Pb) Compounds. *Journal of Electronic Materials*, *51*(7). https://doi.org/10.1007/s11664-022-09659-8.

Schreiber, E., Anderson, O. L., Soga, N., & Bell, J. F. (1975). Elastic Constants and Their Measurement. *Journal of Applied Mechanics*, *42*(3). https://doi.org/10.1115/1.3423687.

Shrikanth, S., Prasad, R., & Neelakantan, S. (2021). Biaxial modulus in fiber-textured thin films: Coinciding Voigt and Reuss bounds and planes of isotropy. *Journal of Applied Physics*, *129*(21). https://doi.org/10.1063/5.0041016.

Waller, I. (1956). Dynamical Theory of Crystal Lattices by M. Born and K. Huang . *Acta Crystallographica*, *9*(10). https://doi.org/10.1107/s0365110x56002370.

Wang, X. T., Dai, X. F., Jia, H. Y., Wang, L. Y., Liu, X. F., Cui, Y. T., & Liu, G. D. (2014). Topological insulating characteristic in half-Heusler compounds composed of light elements. *Physics Letters, Section A: General, Atomic and Solid-State Physics*, *378*(22–23). https://doi.org/10.1016/j.physleta.2014.04.013.

Yadav, M. K., & Sanyal, B. (2015). First principles study of thermoelectric properties of Li-based half-Heusler alloys. *Journal of Alloys and Compounds*, *622*. https://doi.org/10.1016/j.jallcom.2014.10.025.

Zaman, S. U., Rahman, N., Arif, M., Saqib, M., Husain, M., Bonyah, E., Shah, Z., Zulfiqar, S., & Khan, A. (2021). Ab initio investigation of the physical properties of Tl based chloroperovskites TlXCl3(X = Ca and Cd). *AIP Advances*, *11*(1). https://doi.org/10.1063/5.0034759.